CHAPTER 3
Material Characterization

3.1 Introduction

To understand the mechanical behavior of any materials or structures, it is essential to have complete description of the materials. The material characterization is required for designing retrofitting/strengthening purpose as well as developing analytical models. In this chapter, the experimental tests carried out for material characterization of masonry, ECC and FRP have been presented in detail.

3.2 Material Properties of Brick Units

The material properties of bricks depend upon the soil used and it varies from place to place. In this study, four different types of bricks locally available in Rajasthan (India) were used. Three of them were burnt clay bricks while the other was concrete brick. These bricks were designated as C1, C2, C3, and C4. The burnt clay bricks were manufactured by manual moulding process and then burning them in kilns. The concrete bricks were made with a mixture of Portland pozzolana cement, sand, coarse aggregate, and water. The damp mixture was then tamped into the mould. Concrete bricks were cured in water for 28 days before use. The approximate sizes of burnt clay bricks and concrete bricks are 230 × 110 × 75 mm (length × width × height) and 200 × 100 × 100 mm, respectively. Frog for burnt clay bricks had dimensions of 150 × 50 × 15 mm, whereas no frog was there for concrete bricks. The isometric views of burnt clay brick and concrete brick are given in Figs. 3.1a and 3.1b, respectively. Compressive strength and water absorption of these bricks were determined as per IS 3495 [137]. Compressive load was applied on the bricks using 1000 kN capacity of Universal Testing Machine (UTM) in displacement control manner at the rate of 0.01 mm per sec until failure occurs. ASTM C-67 [138] was adopted to determine the initial rate of absorption (IRA) of bricks. The average compressive stress-strain response of these bricks is shown in Fig. 3.2. This respons was obtained from the average data of five sample of each type of brick and error bars for the same are included. Errors bars are graphical representations of the variety of data and used on graphs to indicate the error or uncertainly in a reported measurement.

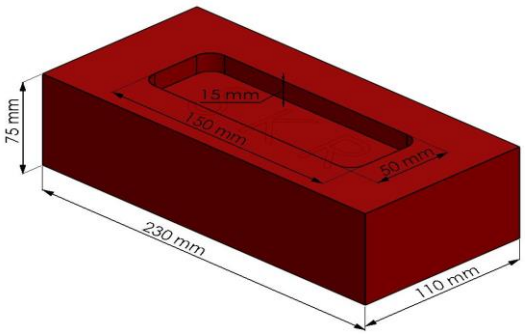

Fig. 3.1 (a) Isometric view of burnt clay brick

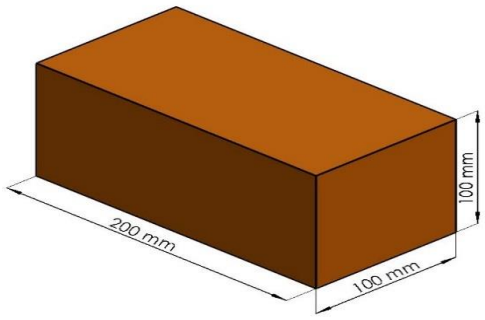

Fig. 3.1 (b) Isometric view of concrete brick

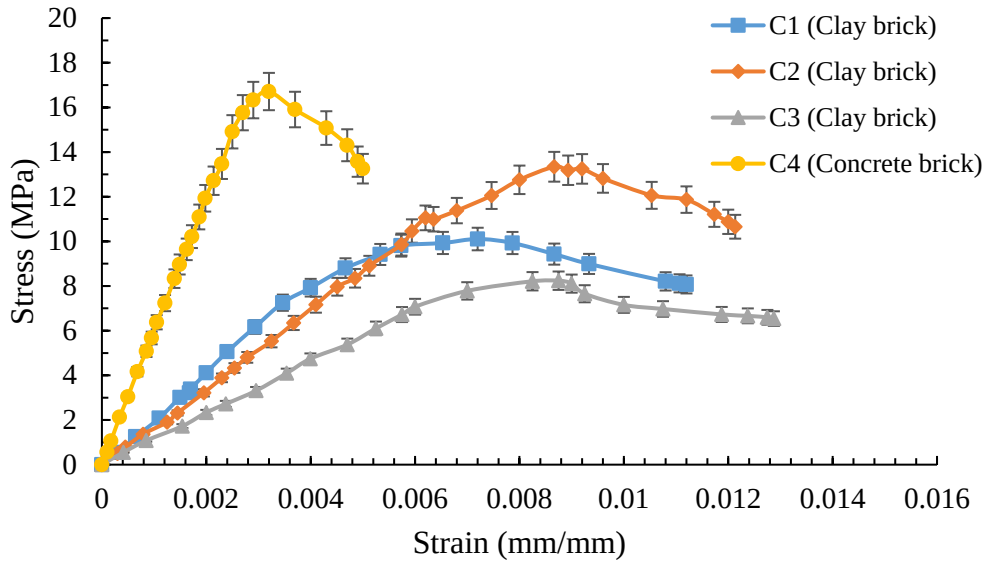

Fig. 3.2 Compressive stress-strain response of brick units

It is seen that for the burnt clay bricks (C1-C3), initially the curve is linear up to about one-third of the ultimate failure stress after which it becomes nonlinear, whereas for the concrete bricks, it is linear up to the peak compressive stress. The material properties such as brick compressive strength (f_b), strain at peak stress, failure strain, and secant modulus of elasticity (E_b) are presented in Table 3.1. The failure strain is defined throughout this chapter as the strain corresponding to stress equal to 80 % of the peak stress in the post peak region. This definition of the failure strain is arbitrary in the sense that after reaching the peak stress, a sudden drop in stress value is observed with small increment in the strain. Thereafter, strain is increasing with higher rate due to crushing of masonry. The modulus of elasticity is defined as secant modulus and it is calculated by measuring the slope between ordinates from 5 to 33% of the ultimate strength of the specimens as

per standard ACI 530-02 [129]. It has been perceived that the secant modulus of elasticity of burnt clay bricks varies between 125 to 200 times of its compressive strength (f_b), whereas for concrete bricks it is observed to be 356 times of compressive strength (f_b) of bricks.

Table 3.1 Physical properties of masonry bricks

Brick design-ation	Brick types	Water absorption, %	Initial rate of absorption (IRA), kg/m^2/min	Max compress-ive strength, MPa	Strain at peak comp. stress, mm/mm	Failure strain, mm/mm	Secant modulus, MPa
C1	Burnt clay	14.42 (10.25)*	3.12 (10.65)*	10.10 (13.25)*	0.0072	0.0111	2001 (14.87)*
C2	Burnt clay	12.19 (15.65)	2.42 (11.87)	13.34 (18.89)	0.0087	0.0121	1705 (23.95)
C3	Burnt clay	13.65 (13.98)	2.74 (13.65)	8.24 (18.26)	0.0088	0.0128	1116 (15.12)
C4	Concre te-brick	7.10 (14.65)	0.75 (12.25)	16.71 (15.87)	0.0032	0.0050	5954 (16.37)

*Value in parentheses represent coefficient of variation in percentage

3.3 Material Properties of Mortar

The compressive strength of cement mortar is considered to be one of the most important aspects of masonry structures. In this study, three mixes consisting of cement: lime: sand proportions (1:0:3, 1:1:4, 1:0:5) were prepared to determine the compressive strength of mortar. Portland pozzolana cement (PPC) as a binder, hydrated lime, and local river sand for the fine aggregate were used to prepare the mortar specimens. Portland pozzolana cement is ordinary Portland cement blended or interground with pozzolanic materials such as fly ash, calcined clay, rice husk ash, etc. Tables 3.2 and 3.3 depict the physical and chemical properties of cement. The fine aggregates passing through 4.75 mm sieve has been used and its particle size distribution is given in Fig. 3.3. The material properties of fine aggregate are given in Table 3.4. The cement mortar mix were prepared in the Hobart mixer for 2-3 minutes of mixing. After mixing the mortar, six cubes of size

(70.7 × 70.7 ×70.7 mm) were cast. A thin layer of release agent was spread on the interiors of the moulds using a clean brush and then a paste of cement mortar was poured into the mould. Excess mortar was struck off with a metallic trowel across the top of the mould. The mould was then placed on the vibrating table and vibrated for 2 minutes at a speed of 12000 ± 400 per minute to achieve full compaction. Specimens were left in the mould inside the room for a period of 24 hours. The specimens were removed from the mould and placed inside the curing tank for 28 days.

Table 3.2 Physical properties of Portland Pozzolana Cement (PPC)

PPC properties	Test results
Blaine fineness (m^2/kg)	375
Specific gravity	3.15
Normal consistency (%)	30.8
Initial and final setting time (Minutes)	28 and 550
% Flyash addition	30
Soundness: Le-chat expansion (mm)	1.00

Table 3.3 Chemical properties of Portland Pozzolana Cement (PPC)

Chemical Composition	Percentage by mass
Calcium oxide (CaO)	43.50
Silicon dioxide (SiO_2)	30.60
Aluminum oxide (Al_2O_3)	10.05
Ferric oxide (Fe_2O_3)	4.32
Alkalies (Na_2O equivalent)	0.56
Magnesium oxide (M_gO)	1.01
Sulfur trioxide (SO_3)	1.95
Loss of ignition (LOI)	2.80
Clinker Analysis	
Tricalcium silicate in clinker (C_3S)	48.5
Dicalcium silicate in clinker (C_2S)	24.5
Tricalcium aluminate in clinker (C_3A)	7.8
Tetracalcium aluminoferrite in clinker (C_4AF)	14.3

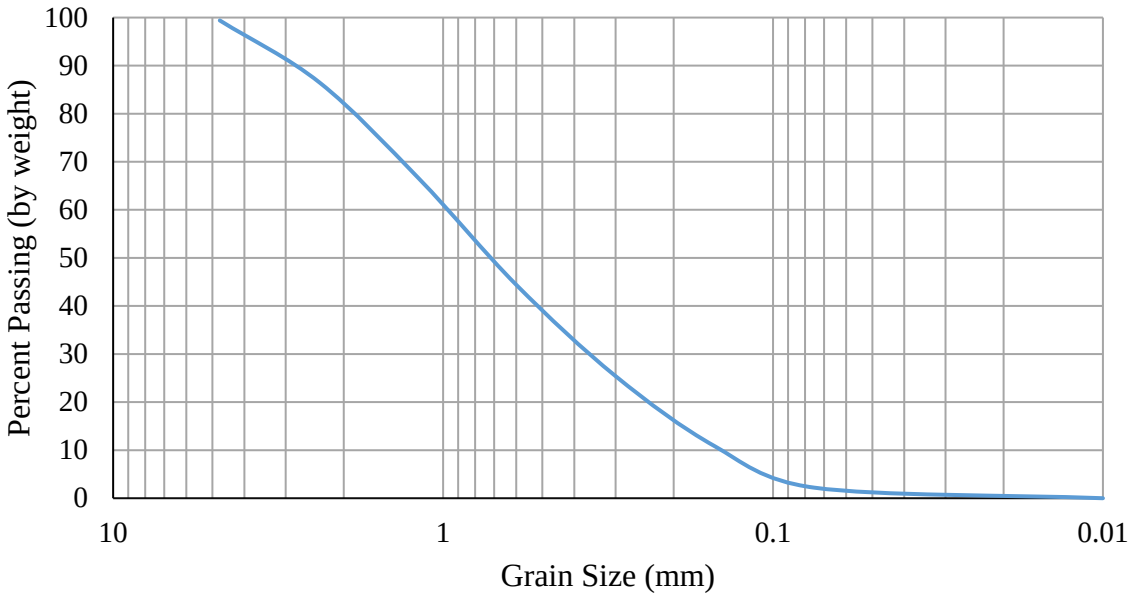

Fig. 3.3 Particle size distribution curve of sand

Table 3.4 Properties of fine aggregates (Sand)

Properties	Values
Fineness modulus	3.5
Specific gravity	2.42
Silt content (%)	2.5
Bulking of sand (%)	22

Six cube specimens were tested for each mix in UTM as per IS 2250 [139] after 28 days. Compressive strength (σ_C) was measured by placing the specimens in the contact of bearing surface of the UTM and the load was applied at the rate of 2-5 N/mm^2 per minute until failure occurs. The compressive strength was calculated by dividing the maximum load applied to the specimen during the test by cross sectional area. The compressive stress-strain response of these mortars is shown in Fig. 3.4. These responses are based on average of six specimens of each mix. As shown in Fig. 3.4, initially the curve is linear up to the peak stress, and then a sudden drop in stress is observed. The average ultimate compressive strength, strain at peak compressive stress, failure strain, and secant modulus of elasticity of mortars are presented in Table 3.5. The secant modulus of elasticity is found to vary between 65 to 80 times of compressive strength of the mortar. The failure pattern of cube specimens subjected to compressive strength test is shown in Fig. 3.5.

In case of cubes under compression test, initial cracks were developed at top and propagated to bottom with increase in load and then the cracks widened at failure along the edge of the cube shown in Fig. 3.5.

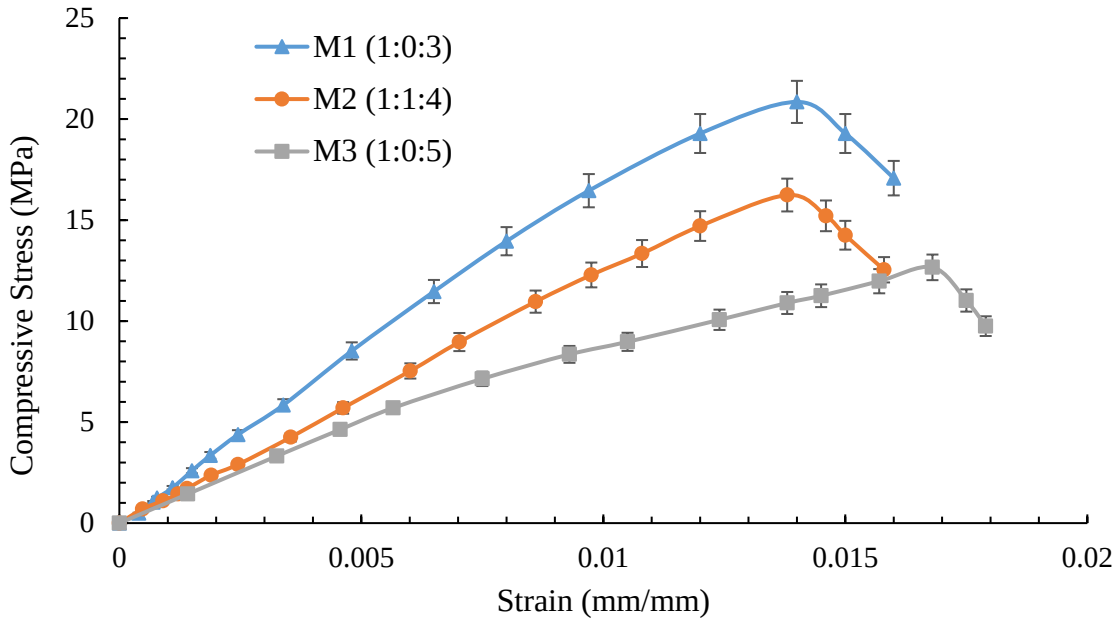

Fig. 3.4 Compressive stress-strain response of mortar

Table 3.5 Physical properties of mortar specimens

Mortar designation	Mortar mix Cement: Lime:Sand	Water/ cement ratio	Cube comp. strength, MPa	Strain at peak comp. stress, mm/mm	Failure strain, mm/mm	Secant modulus, MPa
M1	1:0:3	0.7	20.85 (1.98)*	0.014	0.016	1805 (4.25)*
M2	1:1:4	0.7	16.24 (4.25)	0.014	0.015	1206 (4.65)
M3	1:0:5	0.8	12.66 (2.68)	0.017	0.018	1015 (5.69)

* Value in parentheses represent coefficient of variation in percentage

Fig. 3.5 Typical cube specimen failure of cement mortar

3.4 Material Properties of Masonry

The properties of masonry vary from the properties of its two constituent elements (i.e., brick and mortar). Four types of bricks and three different types of mortars (presented in Sections 3.2 and 3.3) have been used to determine the properties of masonry. The mechanical properties such as compressive strength, stress-strain behavior, modulus of elasticity, and bond strength (flexural and shear) are determined experimentally by combination of four different types of brick and three different types of mortar. These properties are useful for mathematical modeling of masonry structures for their linear and nonlinear responses.

3.4.1 Masonry specimen preparation

A total of 120 masonry prisms were fabricated using combination of each kind of brick and three types of mortar to determine the compressive strength and flexural bond strength of the masonry. The masonry prisms were cast with five bricks stack bonded with specific types of mortar. The thickness of mortar was maintained from 10 to 12 mm. The size of burnt clay brick masonry and concrete brick masonry prisms are 230 × 110 × 423 mm and 200 × 100 × 540 mm, respectively. The typical view of burnt clay brick masonry and concrete brick masonry prisms are shown in Fig. 3.6 (a) & 3.6 (b), respectively. Moreover, masonry triplets were cast with each kind of brick and mortar to determine the shear bond strength of masonry. Each triplet was cast with three bricks and 12 mm thick mortar. Burnt clay bricks prism & triplets were immersed in water for 24 hours before manufacturing, to avoid the absorption of water from the fresh mortars. Masonry prisms and triplets were cured in moist conditioning by wet jute bag for 28 days.

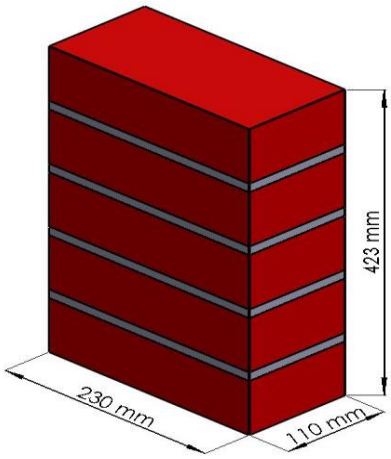

Fig. 3.6 (a) Isometric view of burnt clay brick masonry prism

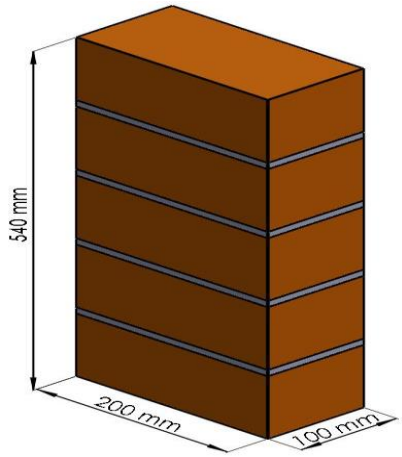

Fig. 3.6 (b) Isometric view of concrete brick masonry prism

3.4.2 Compression strength of prism

The brick masonry prisms were tested as per the procedure given in ASTM C1314-00a [140]. Masonry prisms were capped using gypsum plaster to ensure a uniform load distribution at the time of testing. Compressive load was applied on the brick masonry prism using 1000 kN capacity of Universal Testing Machine (UTM) in displacement control manner at the rate of 0.03 mm per sec until failure occurs. A steel plate of thickness 15 mm was placed at the top and bottom of the prism for uniformly distributed load on the masonry prism while testing. The compressive strength (f_m) of masonry prism was calculated by dividing the maximum compressive load applied to the specimen during the test by cross sectional area.

The average compressive strength of five brick masonry prism specimens including nomenclature, prism strength (f_m), strain at peak stress, failure strain, and secant modulus of elasticity (E_m) are presented in Table 3.6. In the table, for the specimens ID PC1M1, the letters P, C1, and M1 refer to the prism, brick type C1, and mortar type M1, respectively. The compressive stress-strain curves for masonry prisms constructed with combination of four types of brick with three different types of mortar are shown in Figs. 3.7-3.10. These responses were obtained from the average data of five sample of each type of brick and error bars for the same are included in the Figs. 3.7-3.10. It may be noted that for the burnt clay bricks masonry prisms (Figs. 3.7-3.9), the response is almost bilinear up to the peak stress. An initial linear trend was followed by another almost linear trend of rapidly increasing strain up to the peak. This behavior may be attributed to the beginning of clay brick cracking and mortar nonlinearities.

Table 3.6 Experimental results of compressive strength test on masonry prisms

Prism ID	Brick type	Mortar mix Cement:Lime: Sand	Max comp. strength, MPa	Strain at peak comp. stress, mm/mm	Failure strain, mm/mm	Secant modulus, MPa
PC1M1	C1	1:0:3	4.43 (22.65)*	0.0038	0.0078	3825 (23.68)*
PC1M2		1:1:4	3.52 (20.65)	0.0032	0.0076	2337 (25.21)
PC1M3		1:0:5	2.62 (24.21)	0.0029	0.0086	2115 (26.85)
PC2M1	C2	1:0:3	5.41 (17.98)	0.0032	0.0069	4213 (24.75)
PC2M2		1:1:4	4.31 (20.32)	0.0034	0.0072	2671 (28.98)
PC2M3		1:0:5	3.38 (15.21)	0.0034	0.0084	2170 (25.74)
PC3M1	C3	1:0:3	3.61 (22.98)	0.0033	0.0053	2544 (23.69)
PC3M2		1:1:4	2.32 (19.65)	0.0026	0.0050	1908 (24.98)
PC3M3		1:0:5	2.07 (18.21)	0.0045	0.0077	1697 (25.98)
PC4M1	C4	1:0:3	11.59 (17.99)	0.0020	0.0060	6123 (24.03)
PC4M2		1:1:4	10.26 (20.06)	0.0028	0.0082	4960 (20.87)
PC4M3		1:0:5	9.05 (24.25)	0.0034	0.0075	3354 (26.37)

* Value in parentheses represent coefficient of variation in percentage

It is observed in Fig. 3.10 that unlike the burnt clay bricks, the response for the concrete brick masonry prisms is linear up to the peak compressive stress. The masonry prisms constructed with M1 (1:0:3) mortar shows more strength than the other mortars (M2 & M3). It is observed that the compressive strength of the masonry prisms increases with the increase in mortar strength along with increase in compressive strength of brick. Most of the burnt clay brick masonry prisms failed due to formation of vertical splitting cracks along their height as shown in Fig. 3.11. The secant modulus of the burnt clay brick masonry prism was observed to vary between 620 to 870 times of compressive strength of prism (f_m) while for concrete brick masonry prism, it was found to be about 370 to 530 times of compressive strength of concrete brick masonry prism (f_m).

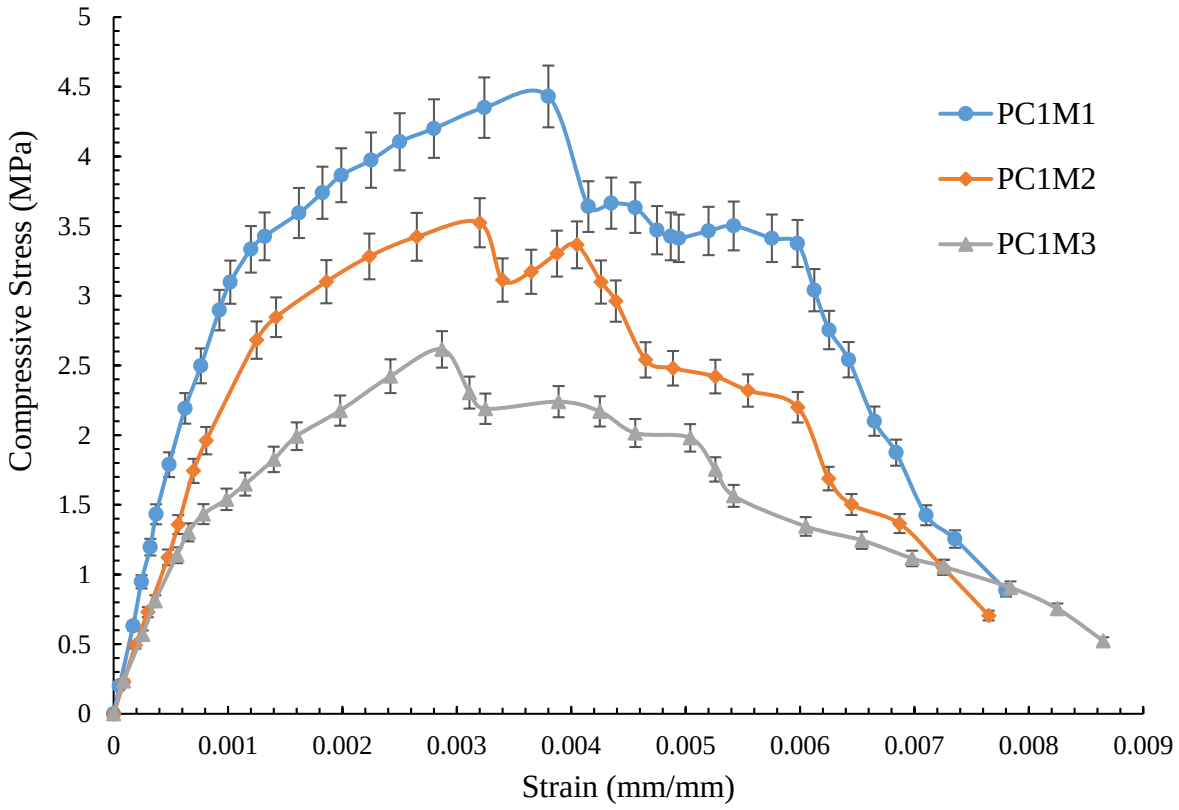

Fig. 3.7 Compressive stress-strain response of masonry prism constructed with C1 brick

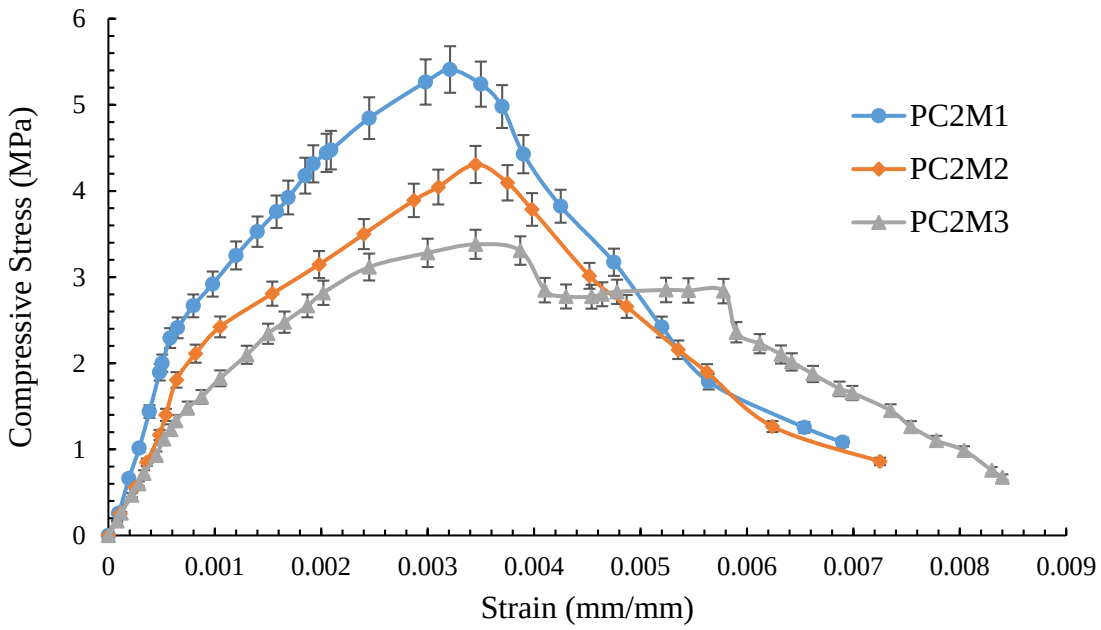

Fig. 3.8 Compressive stress-strain response of masonry prism constructed with C2 brick

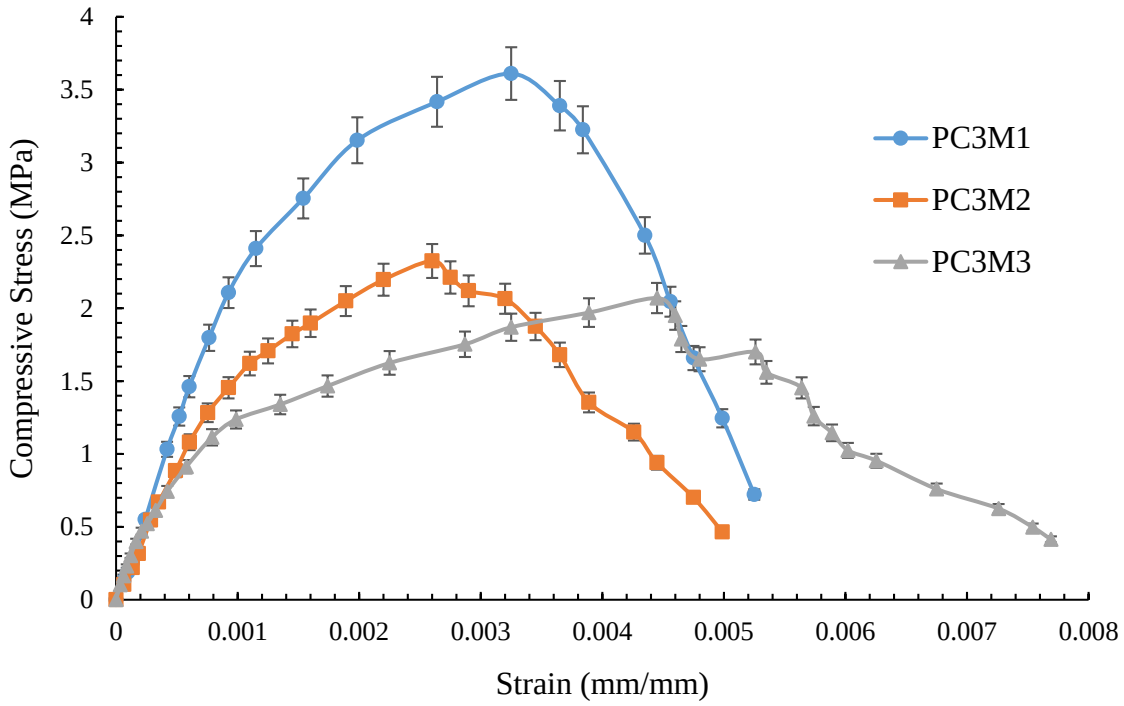

Fig. 3.9 Compressive stress-strain response of masonry prism constructed with C3 brick

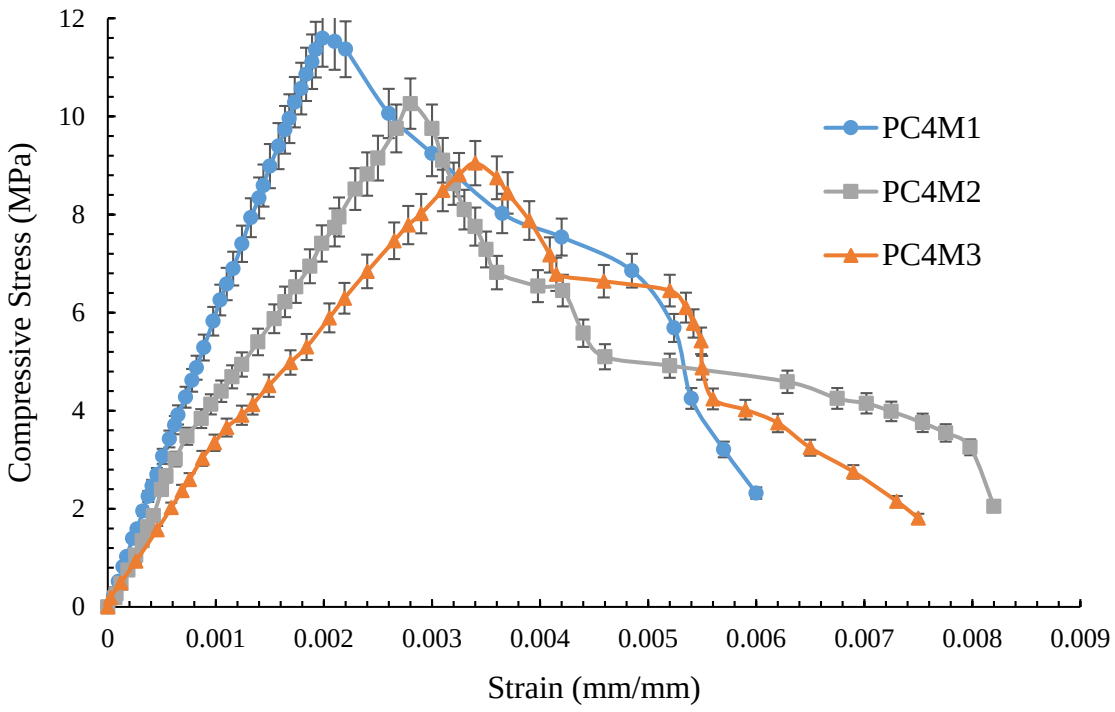

Fig. 3.10 Compressive stress-strain response of masonry prism constructed with C4 brick

Fig. 3.11 Failure pattern of burnt clay brick masonry prism

3.4.3 Flexural and shear bond strength

Flexural bond strength (F_{bs}) of the masonry prisms was determined by testing of five brick prism using a bond wrench test apparatus (Fig. 3.12). The flexural bond strength of masonry prisms was tested as per the procedure given in ASTM C1072 [141]. The schematic diagram of flexural bond strength test is shown in Figs. 3.12a-b. The masonry prism was loaded to failure by incrementally increasing the mass of lever arm in such a way that it failed within 1 to 3 minutes. The failure load of masonry prism was observed and bond strength of masonry parallel to the bed joint is calculated using Eq. 3.1 as per the ASTM C1072 [141] standards.

$$F_{bs} = \frac{6\left(PL_1 + P_1L_2\right)}{b_c d_c^2} - \frac{\left(P + P_1\right)}{b_c d_m} \tag{3.1}$$

where,

F_{bs} = Flexural bond strength (MPa)

P = Maximum applied load (N)

P_1 = Weight of loading arm (N)

L_1 = Distance from center of prism to loading point (mm)

L_2 = Distance from center of prism to centroid of loading arm (mm)

b_c = Cross-sectional width of the mortar-bedded area

d_m = Cross-sectional depth of the mortar-bedded area

The brick masonry triplet specimens were used to determine the shear bond strength of masonry. In this test, vertical movement of the side bricks was restrained and the middle brick was free to move vertically. Vertical load was applied gradually using the servo hydraulic actuator of capacity 200 kN till the failure of bond joint between brick and mortar. The schematic diagrams of shear bond strength test of burnt clay brick and concrete brick triplet are shown in Fig. 3.13 (a) and Fig. 3.13 (b), respectively. The frog area was considered in the case of burnt clay brick for calculation of shear bond strength. Shear bond strength of masonry triplet was calculated using Eq. 3.2 [142].

$$\tau_{bs} = \frac{P}{A_1 + A_2} \tag{3.2}$$

where,

τ_{bs} = Shear bond strength of the masonry

P = Maximum load applied by the machine

A_1 = Area of left side joint

A_2 = Area of right side joint

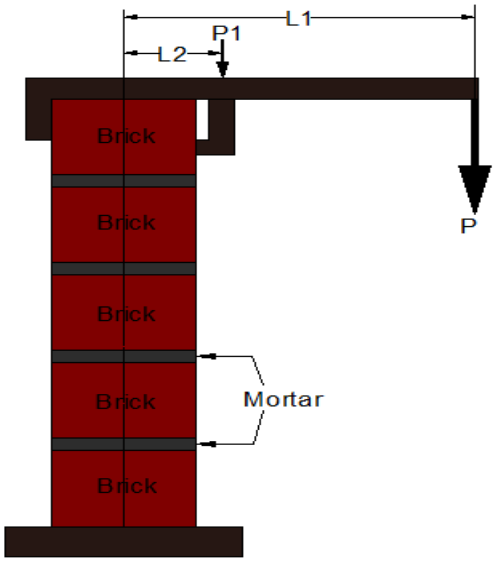

Fig. 3.12 (a) Schematic diagram of flexural bond strength test

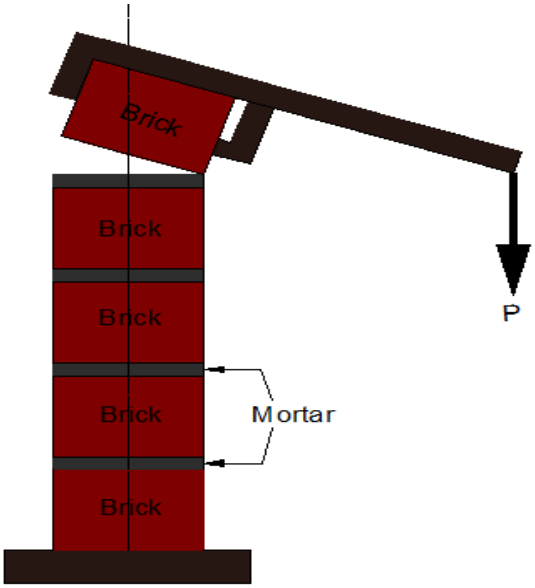

Fig. 3.12 (b) Schematic diagram of failure of masonry prism after bond strength test

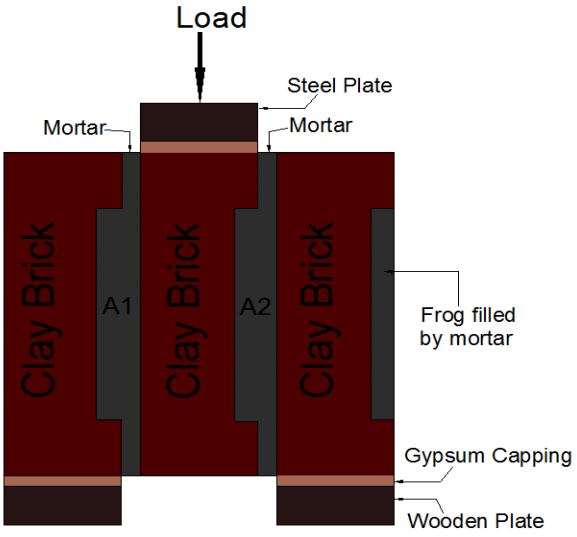

Fig. 3.13 (a) Schematic diagram of shear bond strength test of clay brick

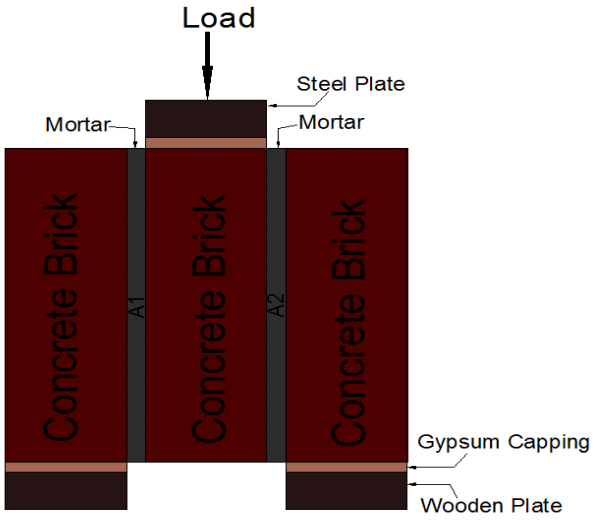

Fig. 3.13 (b) Schematic diagram of shear bond strength test of concrete brick

The average flexural and shear bond strengths of the masonry are presented in Table 3.7. Three types of failure patterns were observed in the burnt clay brick masonry under the flexural and shear bond strength test.

Type A: failure at the brick mortar joint interface as shown in Fig. 3.14 (a)

Type B: failure of brick due to development of crack as shown in Fig. 3.14 (b)

Type C: failure of combination of bond and brick as shown in Fig. 3.14 (c)

Table 3.7 Experimental results of flexural and shear bond strengths

Brick type	Mortar mix Cement: Lime: Sand	Flexural bond strength, MPa	Shear bond strength, MPa
C1	1:0:3	0.201 (28.65)*	0.154 (35.24)*
	1:1:4	0.158 (30.87)	0.129 (32.32)
	1:0:5	0.119 (25.12)	0.090 (27.65)
C2	1:0:3	0.215 (29.98)	0.169 (34.98)
	1:1:4	0.174 (30.54)	0.141 (25.68)
	1:0:5	0.127 (24.25)	0.107 (24.35)
C3	1:0:3	0.184 (25.32)	0.118 (30.21)
	1:1:4	0.134 (26.12)	0.103 (26.45)
	1:0:5	0.095 (30.59)	0.060 (27.65)
C4	1:0:3	0.082 (29.32)	0.042 (28.25)
	1:1:4	0.067 (33.39)	0.031 (29.21)
	1:0:5	0.002 (32.12)	0.001 (28.87)

* Value in parentheses represent coefficient of variation in percentage

Burnt clay brick masonry prisms and triplets constructed with mortar M3 (1:0:5) have shown low flexural and shear bond strength with Type A failure pattern. High strength mortars M1 (1:0:3) & M2 (1:1:4) have shown strong bonding between brick and mortar interface and led to either failure of brick (type B) or a combination of bond and brick failure (Type C). In the concrete brick

masonry, type A failure pattern was observed in all the specimens under flexural as well as shear bond strength tests. The concrete brick masonry has shown poor bond (flexural and shear) strength. It may be attributed to the lesser contact area at the brick-mortar interface. Higher bond strength in burnt clay bricks is found due to the presence of frog (Fig. 3.13a). The bond strength of the concrete brick (Fig. 3.13b) could be improved with increased contact area by providing the frog in the concrete bricks.

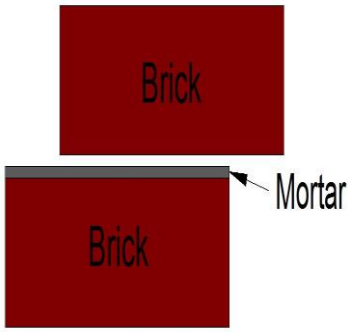

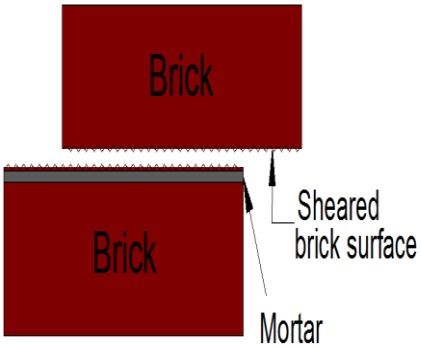

Fig. 3.14 (a) Type A failure **Fig. 3.14 (b) Type B failure** **Fig. 3.14 (c) Type C failure**

3.5 Material Properties of ECC

Engineered Cementitious Composite (ECC) is cement based composite which contain discontinuous short polymeric fibers featuring high ductility and strain hardening behavior based upon micromechanics. ECC can be developed with a variety of polymeric fibers such as polyvinyl alcohol (PVA), polyethylene fiber (PE), and polyester fibers. In this study, two types of polymeric fibers (i.e., polyvinyl alcohol (PVA) fibers and polyester (Poly) fibers) were used for making of ECC. The uniaxial compressive, uniaxial tensile, and four-point bending test were carried out to characterize the mechanical behavior of PVA-ECC and Poly-ECC with same mix proportions.

3.5.1 Materials and mix design

ECC generally consists of mixtures of cement, silica-sand, Fly-ash, water, super-plasticizer, and polymeric fibers to reinforce the mix. In this study, Portland pozzolana cement (PPC) as binder, micro silica sand with an average grain size of 100 µm, and class F fly-ash (Pozzocrete-63) was used to prepare the ECC. The material properties of Portland pozzolana cement is presented in Tables 3.2-3.3. Master Glenium Sky 8777 provided by BASF India Ltd. was used as the super plasticizer. This superplasticiser is based on second generation polycarboxylic ether polymers,

developed using Nano-technology and compatible with all types of cement. The material properties of the superplasticizer provided by manufacturer are briefly presented in Table 3.8. The present study used two types of polymeric fibers such as polyester fibers of triangular shape and polyvinyl alcohol (PVA) fibers. The material properties of polymeric fibers provided by manufacturer are given in Table 3.9. The mix proportion of ECC used in this study has been taken from literature [32] and presented in Table 3.10.

Table 3.8 Materials properties of super-plasticizer [143]

Properties	Polyester fiber
Aspect	Light brown liquid
Relative density	1.10 ± 0.01 at 25° C
pH	≥6
Chloride ion content	< 0.2 %

Table 3.9 Materials properties of polymeric fibers

Properties	Polyester fiber	PVA fiber
Fiber diameter (mm)	0.025-0.035	0.04
Fiber length (mm)	12	8
Aspect Ratio (length/dia)	342-480	200
Tensile strength (MPa)	480	1600
Elongation (%)	30	-
Rupture strain (%)	-	7
Manufacturer by	Reliance, India	Kuraray & Co., Japan

Table 3.10 Mix proportion of ECC in kg/m^3

Cement	Silica sand	Fly-ash	Water	Super plasticizer	Fiber
620 kg/m^3	620 kg/m^3	620 kg/m^3	290 kg/m^3	8.5 kg/m^3	26 kg/m^3

3.5.2 Mixing process and specimen preparations

Hobart mixer (Fig.3.15) was used to prepare the ECC. The mixing process is completed in the three steps.

Step 1: Water and super plasticizer are added and thoroughly mixed using Hobart mortar mixer.

Step 2: Silica sand is then added and is mixed for around 2 minutes. Then Fly-ash is added and the mixing process is continued.

Step 3: Further cement is added and mixed about 5 minutes. Fibers are then added slowly. The entire process takes around 20-25 minutes. In this mixing method, cement is added in the step 3 because entire process will take around 20-25 minutes, since cement would attain its initial setting time in this period.

After mixing the ECC, cubes of size 150 × 150 × 150 mm and 70.7 × 70.7 × 70.7 mm, cylinders of size 150 × 300 mm and 100 × 200 mm, ECC sheet of size 600 × 350 × 13 mm (for tensile coupons), and rectangular prisms of size 100 × 100 × 500 mm were cast. A thin layer of release agent was spread on the interiors of the moulds using a clean brush and then a paste of ECC was poured into the mould. Specimens were left in the mould inside the moist room for a period of 24 hours. The specimens were removed from the mould and placed inside the curing tank at temperature of 27 ± 3 °C for 28 days. ECC specimens were divided into two categories i.e., PVA-ECC and Poly-ECC as differentiated with type of the fibers inclusion.

Fig 3.15 Mixing of standard ECC mixture ingredients using Hobart mixer

3.5.3 Compressive strength of ECC

For analyzing compressive strength of ECC, cylindrical and cube specimens were tested using Compression Testing Machine (CTM) of capacity 2000 kN after 28 days. Five cylindrical specimens of size 150 × 300 mm and five cube specimens each of size 150 × 150 × 150 mm and 70.7 × 70.7 × 70.7 mm were tested. Cylindrical and cube specimens were tested as per ASTM C39 [144] and IS 516 [145], respectively. Compressive strength was measured by placing the specimens in the contact of bearing surface of the CTM and the load was applied at the rate of 2-5 N/mm^2 per minute until failure occurs. The compressive strength was calculated by dividing the maximum load applied to the specimen during the test by cross sectional area. The modulus of elasticity and Poisson's ratio of cylindrical specimens were calculated using Eqs. 3.3 and 3.4 [146], respectively. The strain was measured by the extensometer attached with the CTM as shown in Fig. 3.16.

$$E_c = \frac{(S_2 - S_1)}{(\varepsilon_2 - \varepsilon_1)} \tag{3.3}$$

$$\mu = \frac{(\varepsilon_{t2} - \varepsilon_{t1})}{(\varepsilon_2 - \varepsilon_1)} \tag{3.4}$$

where,

E_c = Chord modulus of elasticity, MPa

S_2 = Stress corresponding to 40 % of ultimate load, MPa

S_1 = Stress corresponding to a longitudinal strain (ε_1), MPa

ε_2 = Longitudinal strain corresponding to stress S_2, mm/mm

ε_1 = 3.45E-7 (longitudinal strain in mm/mm)

μ = Poisson's ratio

ε_{t2} = Transvers strain at mid-height of the specimens produced by stress S_2, mm/mm

ε_{t1} = Transvers strain at mid-height of the specimens produced by stress S_1, mm/mm

Fig. 3.16 Failure pattern of cylindrical specimen

The results of compressive strength, strain at peak stress, failure strain, and modulus of elasticity are presented in Table 3.11. The failure strain is defined as the strain corresponding to stress equal to 80 % of the peak stress in the post peak region. This definition of the failure strain is arbitrary in the sense that after reaching the peak stress, a sudden drop in stress value is observed with small increment in the strain. Thereafter, strain is increasing with higher rate due to crushing of ECC. The average compressive strength of cube (150 mm), cylinder (150 × 300 mm), and small cube (70.7 mm) specimens is observed to be 54.05, 45.12, and 61.74 MPa, respectively for PVA-ECC whereas it is found to be 46.25, 38.55, 50.88 MPa, respectively for Poly-ECC. The compressive strengths of cylinder (150 × 300 mm), and small cube (70.7 × 70.7 × 70.7 mm) are observed to be 0.83 and 1.14 times of compressive strength of standard cube (150 × 150 × 150 mm), respectively for PVA-ECC whereas they are observed to be 0.83 and 1.10 times of compressive strength for Poly-ECC. The compressive strength of PVA-ECC is found to be 1.17 times of the compressive strength of Poly-ECC. The compressive axial stress-strain response of the cylindrical specimens

of ECC (PVA-ECC and Poly-ECC) is shown in Fig. 3.17. It is seen that, initially both the curves are linear up to about half of the peak stress after which it becomes nonlinear accompanied by a sudden drop in the stress is observed after peak load. The failure pattern of cube specimen is shown in Fig. 3.18. It has been observed that vertical axial cracks develop in the most of the specimens (Fig. 3.18). In case of cylinder specimens under compression test, initial cracks developed at top and propagated to the bottom with increase in load and then the cracks got widened at failure along the top of the specimen as shown in Fig. 3.16.

Table 3.11 Experimental results of compressive strength and split tensile strength tests

ECC types	Cube[a]	Cube[b]	Cylinder, 150 × 300 mm					Cylinder, 100 × 200 mm
	Comp. strength, MPa	Comp. strength, MPa	Comp. strength, MPa	Peak comp. strain, mm/mm	Failure strain[c], mm/mm	Comp. modul-us GPa	Poisson's ratio	Split tensile strength, MPa
Poly-ECC	46.25	50.88	38.55	0.0030	0.0031	16.85	0.164	3.81
PVA-ECC	54.05	61.74	45.12	0.0032	0.0033	22.24	0.172	4.24

Cube[a] = size of cube is 150 × 150 × 150 mm

Cube[b] = size of cube is 70.7 × 70.7 × 70.7 mm

Failure Strain[c] = strain corresponding to stress equal to 80 % of the peak stress in the post peak region

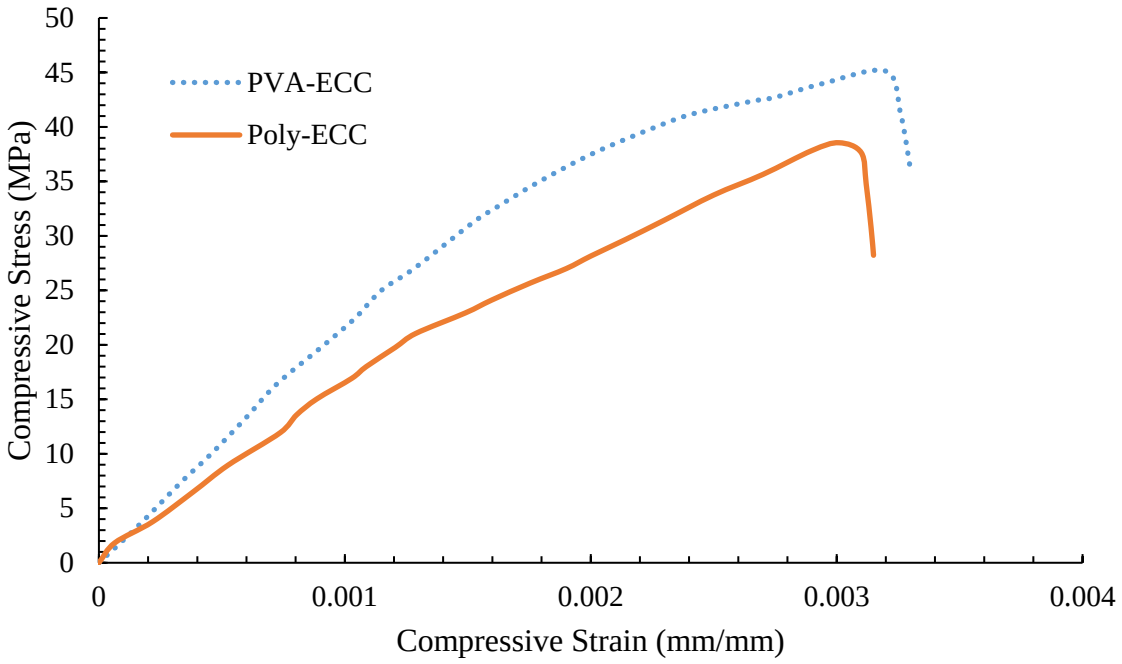

Fig. 3.17 Compressive stress-strain response of ECC cylinder specimens

Fig. 3.18 Failure pattern of cube specimen

3.5.4 Split tensile strength

The split tensile strength of ECC was measured through testing of five cylindrical specimens (100 × 200 mm) of each category as per IS 5816 [147] and BS 1881-part 117 [148]. The split tensile strength can be calculated using Eq. 3.5. In this Eq., f_{ct} is split tensile strength, P is the load applied to the specimen, and l, d_a are length and diameter of the specimen, respectively.

$$f_{ct} = \frac{2P}{\pi d_a l} \tag{3.5}$$

The results of split tensile strength of ECC are presented in Table 3.11. Failure modes of split tensile strength test of cylindrical specimens are shown in Fig. 3.19. It is observed that, cylinder specimens got split into two pieces as shown in Fig. 3.19.

Fig. 3.19 Failure pattern of cylindrical specimen after split tensile strength test

3.5.5 Tensile strength of ECC coupons

Five specimens of ECC coupons of each category were tested in automated deformation controlled hydraulic Universal Testing Machine (UTM) of capacity 100 kN and the load was applied at displacement control rate of 0.5 mm/min. The ECC coupons of size 310 × 75 × 13 mm was extruded from the ECC sheet using marble cutter. The gauge length was maintained as 200 mm. The tensile stress-strain response of ECC coupons were measured by the UTM. The results of tensile strength of ECC coupons are presented in Table 3.12. The failure pattern of Poly-ECC coupon during the tensile strength test is shown in Fig. 3.20. All the coupons have shown multiple cracking and pseudo strain hardening behavior. After the first crack, load is continued to rise without fracture. Subsequently, parallel cracks are developed and the crack width increases with increasing stress. The average tensile stress-strain response of the ECC coupons is presented in Fig. 3.21. It is seen that PVA-ECC has higher tensile strength in comparison to the Poly-ECC. The tensile strength of PVA-ECC is about 2 times of tensile strength of Poly-ECC. After the first crack, the tensile stress is increased in PVA-ECC due to bridging action of cement and fibers bonding whereas in Poly-ECC, small drop in stress is observed after the first crack and then, stress increases due to strain hardening. The reason behind this significant strength in PVA-ECC is PVA fiber

which has higher tensile strength and stronger bonding with cement matrix in comparison to Polyester fibers.

Table 3.12 Experimental results of tensile strength of ECC coupons

Properties	Poly-ECC	PVA-ECC
Tensile strength, MPa	2.51	4.78
Peak strain, %	0.04	0.20
Rupture strain, %	2.40	2.80
Young's modulus, GPa	8.20	9.60

Fig. 3.20 Failure pattern of ECC coupon during tensile strength test

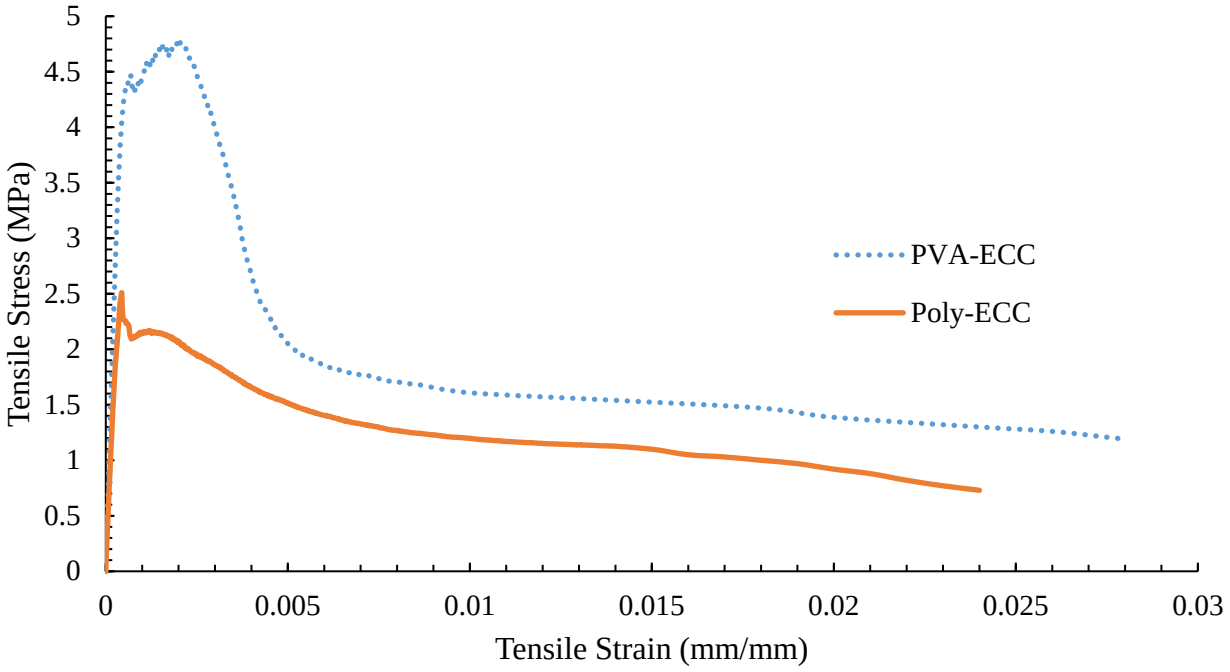

Fig. 3.21 Average tensile stress-strain response of ECC coupons

3.5.6 Bending test of ECC prism

Four-point bending tests were performed on the five rectangular prism specimens of each category on servo hydraulic actuator of capacity 200 kN as per ASTM D790 [149]. The load was applied on the prisms at the displacement control rate of 0.5 mm/min. The flexural stress, strain and modulus were calculated using Eqs. 3.6-3.8, respectively.

$$\sigma_f = \frac{PL}{bd^2} \tag{3.6}$$

$$\varepsilon_{fo} = \frac{6Dd}{L^2} \tag{3.7}$$

$$E_{bn} = \frac{L^3 m}{4bd^3} \tag{3.8}$$

where,

σ_f = Flexural stress, MPa

P = Load at a given point on the load-deflection curve

L = Support span, mm

b = Width of the specimen, mm

d = Depth of specimen, mm

ε_{fo} = Flexural strain in the outer surface, mm/mm

D = Maximum deflection of the axis of the beam, mm

E_{bn} = Modulus of elasticity in bending, MPa

m = Slope of the tangent to the initial portion of the load deflection curve, N/mm

The results of the four-point bending test of ECC prisms are presented in Table 3.13. The average flexural strength of PVA-ECC and Poly-ECC is observed to be 9.49 and 8.52 MPa, respectively. The average peak flexural strain of PVA-ECC is 0.017 whereas it is found to be 0.016 for Poly-ECC. The flexural stress-strain response of the ECC prism is presented in Fig. 3.22. PVA-ECC prism has shown more flexural stress in comparison to Poly-ECC. The flexural strength of PVA-ECC prism is found to be 1.11 times of the flexural strength of Poly-ECC prism. The failure pattern of ECC prism during four-point bending test is shown in Fig. 3.23. The vertical flexural cracks developed in the tension zone and propagated towards the compression zone as shown in Fig. 3.23.

Table 3.13 Experimental results of bending test of ECC prism

Properties	**Poly-ECC**	**PVA-ECC**
Flexural strength, MPa	8.52	9.49
Peak strain, %	1.59	1.68
Failure strain, %	1.60	1.73
Flexural modulus, MPa	98.74	83.15

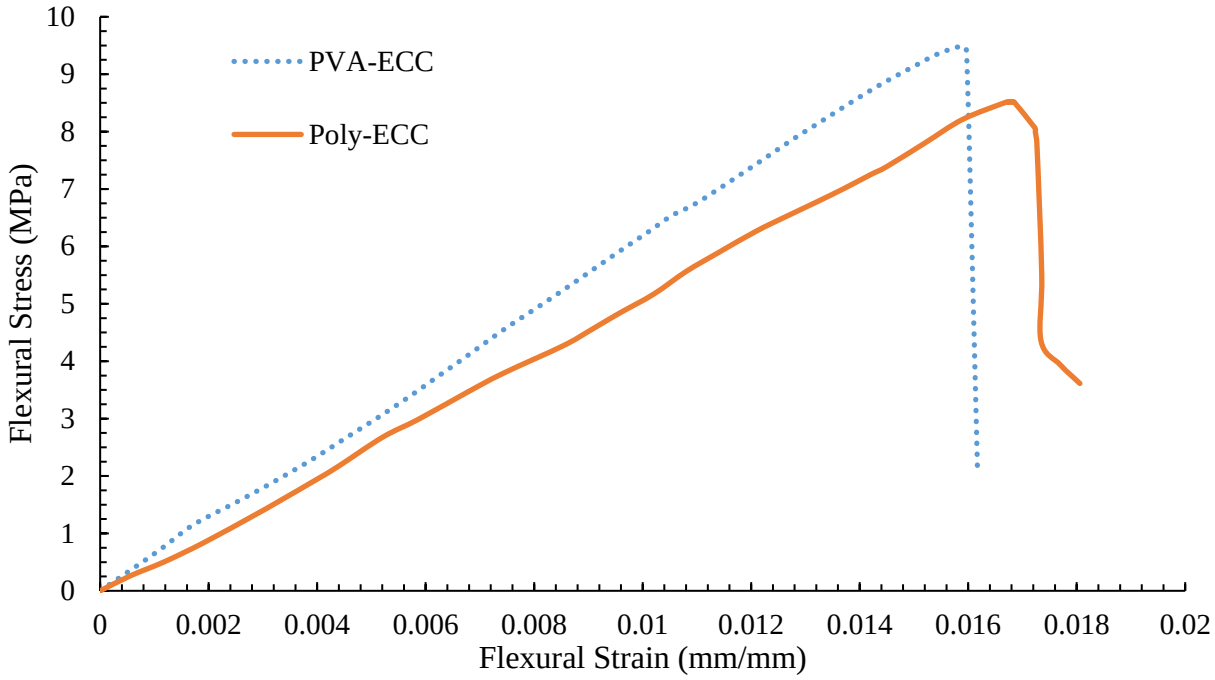

Fig. 3.22 Flexural stress-strain response of ECC prism

Fig. 3.23 Failure of ECC prism during four-point bending test

3.6 Material Properties of FRP

The study of material characterization of FRP is very important for its application in strengthening and retrofitting of structures. The properties of FRP varies from manufacturer to manufacturer; therefore, it is necessary to predict the material characterization of FRP using suitable test methods. In this study, three types of fibers (i.e., glass, carbon and basalt) were used for strengthening purpose. The uniaxial tensile tests were carried out to characterize the basic required properties of glass, carbon and basalt fibers for strengthening purpose.

3.6.1 FRP specimen preparations

FRP sheet were manufactured by manually impregnating dry fibers with thermosetting resin (epoxy). Epoxy (resin) of grade 'Resin 691' and hardener of grade 'Reactive Polyamide 140' was used for making the paste. Resin was used having viscosity of 7000-10000 mPas and hardener of viscosity 6000-7000 mPas. Mixture of resin and hardener was made with proportion of 85:15 by weight as described by the manufacturer. The glass, carbon and basalt FRP sheet of size 300 × 300 mm were fabricated as per as per standard ASTM D7565/D7565M-10 [150]. The volume fraction of fiber and resin were maintained 60-65 % and 35-40 %, respectively. The FRP sheets were left for air curing at room temperature for 15 days before testing.

3.6.2 Uniaxial tensile strength of FRP

To predict the basic mechanical properties such as tensile strength and Young's modulus, tensile tests were performed as per ASTM D3039 [151]. Five rectangular coupons of approximate size 250 × 25 × t mm were extruded from FRP sheet using "Power hack saw" machine, where thickness "t" varied from specimen to specimen. The tests were performed in automated deformation controlled hydraulic Universal Testing Machine (UTM) of capacity 100 kN and the load was applied at displacement control rate of 2 mm/min. The gauge length was maintained as 150 mm while 50 mm grip length was provided on either end of the specimens. The ends of the coupons were pasted with emery paper and securely fastened in between the wedge grips. The hydraulic oil pressure was maintained in such a way that no slippage and breakage occurred of the coupons inside the grips. It was ensured that coupons are perfectly straight while placing the specimens inside the grips as shown in Fig. 3.24. The tensile stress-strain response of coupons was recorded via a data acquisition system and report was generated on a computer. The average stress-strain response obtained from tensile test are shown in Fig. 3.25 The behavior of tensile stress-strain response of the FRP is bi-linear. Young's modulus was calculated from the first linear portion of stress–strain response. The tensile strength properties of the FRP is given in Table 3.14.

Fig. 3.24 Tensile testing of CFRP coupon

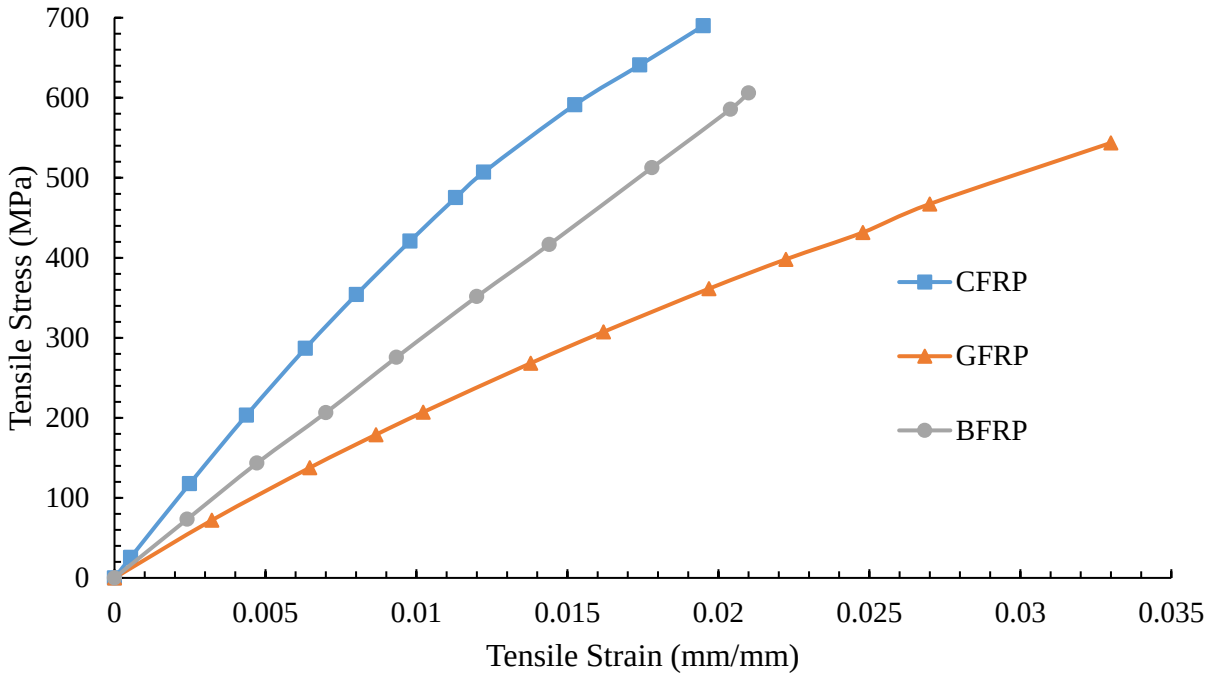

Fig. 3.25 Average tensile stress-strain response of FRP coupons

Table 3.14 Mechanical properties of FRP

FRP Type	Thickness (mm)	Ultimate tensile strength (MPa)	Ultimate strain (%)	Young's modulus (GPa)
Carbon fabric dry	0.44	1697	1.47	104
Glass fabric dry	0.65	1077	2.25	66
Basalt fabric dry	0.38	1495	1.85	82
CFRP* Laminate	2.00	690	1.90	46
GFRP** Laminate	2.43	543	3.30	18
BFRP*** Laminate	2.00	606	2.10	39

*CFRP = Carbon fiber reinforced polymer

**GFRP = Glass fiber reinforced polymer

***BFRP = Basalt fiber reinforced polymer

3.6.3 FRP bars

In this study, two types of FRP bars were used. The first type was manufactured by pultrusion process, supplied by ZOLTEK, India (Manufacturers Company). Type 2 was fabricated locally by hand lay-up process using mechanically developed specialized twisting equipment as shown in Fig.3.26. In this equipment, hooks are connected to the handle at the ends of the equipment, and fiber rovings are tensioned between the hooks. Fibers are impregnated with epoxy adhesive. After tensioning the fiber between two ends, hooks are rotated for outward twisting. This way the fibers also get entangled with each other and then get stretched outward causing excess resin to drip out as shown in Fig.3.27. This also helps in maintaining uniform bar diameter without sagging. After the proper number of rotations, the hooks and handles are fixed, and the entire set is left to cure. The FRP bar is cut from the ends after 72 hours. The typical length and diameter of the CFRP bars is 1.5 m and 8 mm, respectively.

Fig. 3.26 Self-developed FRP bar manufacturing equipment

Fig. 3.27 Fabrication of CFRP bar

3.6.4 Tensile strength of FRP bars

The tensile tests of FRP bars were carried out in accordance with ASTM D7205/D7205M [152]. For the tensile testing of FRP bars, an anchorage system consisting of steel pipe of diameter 38 mm filled with an expansive grout cement (CICO GROUT-V1) was used to avoid premature failure within the grip zones. The grout cement (CICO GROUT-V1) filled into the steel pipe have

cured for four weeks to obtain the compressive strength of approximately 75 MPa. The total length of the specimen was 1300 mm and the gauge length was 380 mm. The schematic diagram of anchorage system is shown in Fig. 3.28. The tests were conducted using UTM with a capacity of 1000 kN and the specimens fixed both at the top and the bottom with the wedge frictional metal grips of the UTM. The load was applied at displacement control rate of 2 mm/min. All the specimens were failed suddenly as expected. Fig. 3.29 shows the failure mode of representative specimens for each bar type. Table 3.15 summarizes the average results of tensile testing of FRP bars used in this study. A total of 15 samples consisting 5 specimens for each bars was tested. The average tensile stress-strain response of FRP bars is shown in Fig. 3.30. It should be noted that all the reported results represent the average of five tested specimens. The stress-strain behavior of FRP bars approximates that of a linear-elastic brittle material and does not yield as shown in Fig. 3.30.

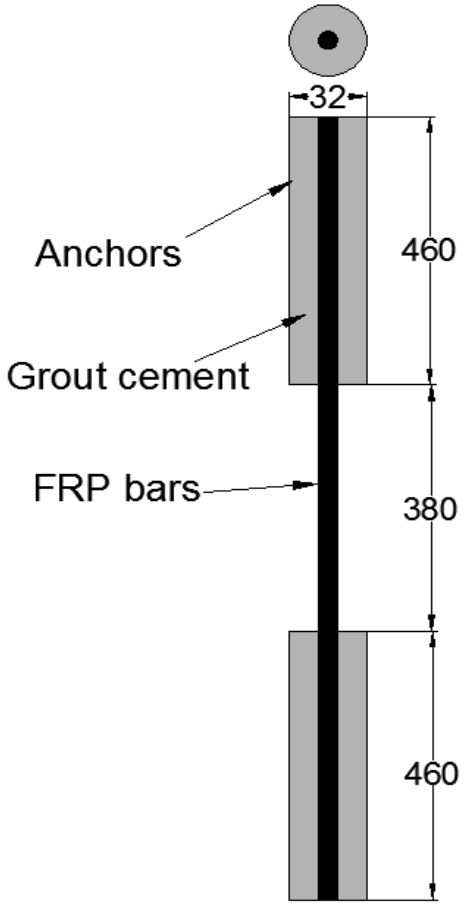

Fig. 3.28 Anchorage system of FRP bars

Fig. 3.29 Typical failure of CFRP bar

Table 3.15 Tensile strength properties of FRP bars

Sr. No	FRP Type	Diameter, mm (Area, mm^2)	Tensile strength (MPa)	Young's modulus (GPa)	Failure strain (%)
1	Pultruded CFRP	8.0 (50.24)	2217	55	2.23
2	Hand lay-up CFRP	8.0 (50.24)	1671	48	2.16
3	Hand lay-up GFRP	8.0 (50.24)	920	23	3.50

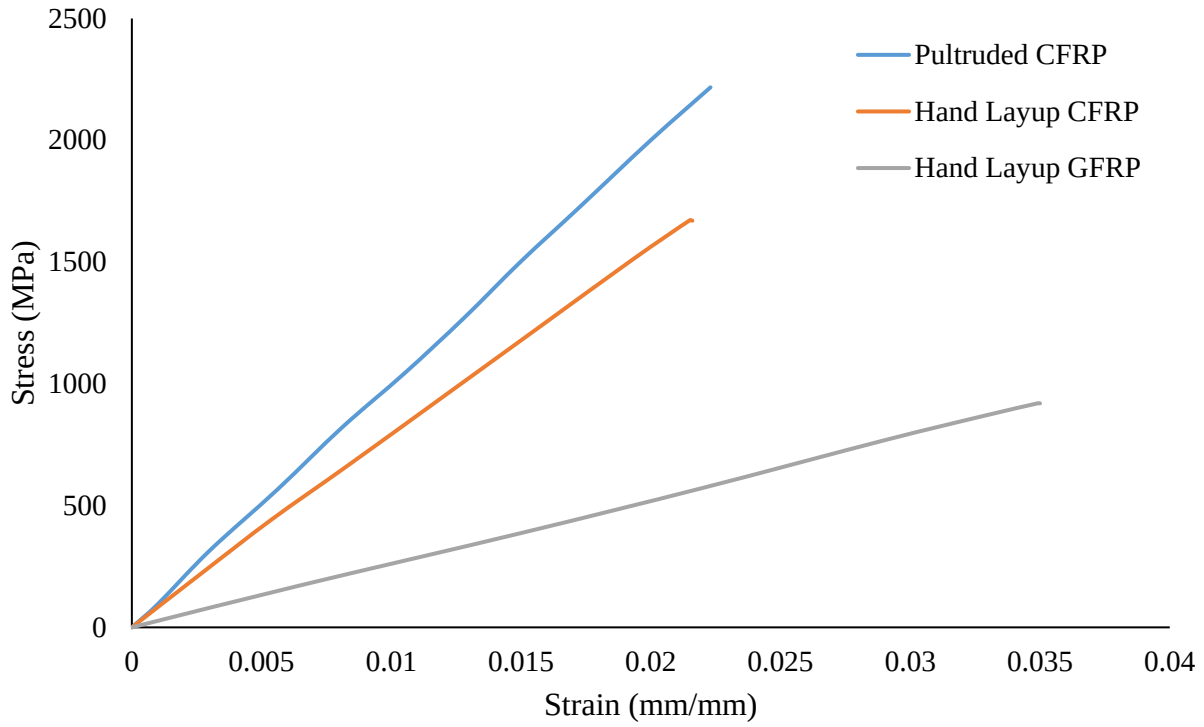

Fig. 3.30 Tensile stress-strain response of FRP bars

3.7 Bonding Material

The SikaDur 330, thixotropic, epoxy based impregnating resin/adhesive was used as a bonding material for strengthening applications. The SikaDur 330 in two-part which is supplied in mix ratio of 4:1 by weight comprising the correct quantities of Part A and Part B. Mixer was prepared thoroughly stirring both components separately until the color of paste changes into light grey. The material properties of Sikadur 330 provided by the manufacturer is given in Table 3.16.

Table 3.16 Properties of SikaDur 330 (Epoxy resin) used for strengthening purpose

Properties	SikaDur 330
Density (kg/lt) at 23°C	1.31
Tensile strength (MPa)	30
Young's modulus (GPa)	4.5
Elongation at break (%)	0.9
Viscosity (mPas) at 23°C	6000
Thermal expansion coefficient per °C	45×10^{-6}

3.8 Concluding Remarks

The experimental study was conducted to determine the basic properties of brick, mortar, masonry, ECC, and FRP. These properties are important for the strengthening of masonry structures using FRP and ECC. The following concluding remarks are made based on the results presented in this Chapter.

- The compressive strength of masonry prism is influenced by the compressive strength of brick and mortar. It increases with the increase of compressive strength of both the bricks and mortar.
- The secant modulus of burnt clay brick masonry and concrete brick masonry is found to vary between 620 to 870 times and 370 to 530 times, respectively of the corresponding masonry prism strength.
- The concrete brick masonry has poor bond strength in comparison to burnt clay brick masonry due to less contact area. However, the concrete brick masonry bond strength could be improved by either providing frog or surface coating with enhanced materials strength.
- The compressive strengths of cylinder specimens (150 × 300 mm) and small cube (70.7 mm) specimens are found to be 0.833 and 1.20 times of the compressive strength of standard cube (150 mm size).
- The compressive, tensile, and flexural strengths of PVA-ECC respectively are found to be 1.14, 2, and 1.11 times of its compressive, tensile and flexural strength of Poly-ECC.

- The compressive, tensile, and flexural modulus of PVA-ECC are found to be 22.24, 9.58, and 0.98 GPa, respectively whereas for Poly-ECC, these are 16.85, 7.50, and 0.83 GPa, respectively.
- New twisting equipment has been developed for the fabrication of FRP bars aimed at small scale strengthening projects. The quality of FRP bars produced by the equipment is excellent in terms of strength and stiffness with respect to small scale strengthening projects.